Influence of intra-yarn flows on whole 3D woven fabric numerical permeability: from Stokes to Stokes-Darcy simulations

Aubin Geoffre, Yanneck Wielhorski, Nicolas Moulin, Julien Bruchon, Sylvain Drapier, Pierre-Jacques Liotier

▶ **To cite this version:**

Aubin Geoffre, Yanneck Wielhorski, Nicolas Moulin, Julien Bruchon, Sylvain Drapier, et al.. Influence of intra-yarn flows on whole 3D woven fabric numerical permeability: from Stokes to Stokes-Darcy simulations. International Journal of Multiphase Flow, 2020, 129, pp.103349. 10.1016/j.ijmultiphaseflow.2020.103349 . emse-02888000

HAL Id: emse-02888000

https://hal-emse.ccsd.cnrs.fr/emse-02888000v1

Submitted on 22 Aug 2022

HAL is a multi-disciplinary open access archive for the deposit and dissemination of scientific research documents, whether they are published or not. The documents may come from teaching and research institutions in France or abroad, or from public or private research centers.

L'archive ouverte pluridisciplinaire **HAL**, est destinée au dépôt et à la diffusion de documents scientifiques de niveau recherche, publiés ou non, émanant des établissements d'enseignement et de recherche français ou étrangers, des laboratoires publics ou privés.

Distributed under a Creative Commons Attribution - NonCommercial 4.0 International License

Version of Record: https://www.sciencedirect.com/science/article/pii/S0301932219309863
Manuscript_8133f8f00a7298f4e9c0c2006e0bb6db

Influence of intra-yarn flows on whole 3D woven fabric numerical permeability: from Stokes to Stokes-Darcy simulations

Aubin Geoffre[a], Yanneck Wielhorski[b], Nicolas Moulin[a,*], Julien Bruchon[a], Sylvain Drapier[a], Pierre-Jacques Liotier[a]

[a] *Mines Saint-Étienne, Université de Lyon, CNRS, UMR 5307 LGF, Centre SMS 158 Cours Fauriel - 42023 Saint-Étienne, France*
[b] *Safran Aircraft Engines, Rond-point René Ravaud, Réau, Site de Villaroche, 77550 Moissy-Cramayel, France*

Abstract

2D and 3D numerical permeability of fibrous media are studied based on Stokes and Stokes-Darcy flows simulated by a Finite Element Modelling (FEM). A monolithic approach stabilised by an Algebraic Sub-Grid Scale (ASGS) method and implemented in a FEM software (Z-set) is used. The 2D geometries have been generated according to ideal arrangements and 3D geometry are representative of a highly anisotropic ply-to-ply interlock unit cell. For both geometries, yarns have been first considered as impermeable, and then the same calculations have been conducted with various intra-yarn permeabilities. The main novelty of this work is to address the dual-scale permeability problem with a Stokes-Darcy modelling so as to override numerical strategy robustness issues. An empirical law has been proposed to link the effective permeability to the intra-yarn one : this allows to generalise previously established results to real 3D materials with complex structures. An intra-yarn permeability threshold (asymptotic value) from which yarns can be considered impermeable has also been highlighted. This study underlines the importance of unit cell definition when it comes to computing permeability of 3D structures numerically generated, especially non-periodicity issues. Two methods to decrease the impact of preferential flows are then discussed.

Keywords: 3D Angle-interlock fabric, Numerical permeability, Flow simulation, Stabilised FEM, Stokes-Darcy coupling

© 2020 published by Elsevier. This manuscript is made available under the CC BY NC user license
https://creativecommons.org/licenses/by-nc/4.0/

1. Introduction

Resin Transfer Moulding (RTM) processes are used for manufacturing composite parts in various industrial sectors (fan blades for aeronautics [1], wind power [2], etc.). This type of process can be divided into two major steps. The first one corresponds to a compression phase of a fibrous preform within a mould until a desired fibre volume ratio V_f is reached [3, 4]. The dry fibrous medium, which can be considered as a porous medium, is then impregnated with a polymer resin under flux or pressure controlled conditions. A detailed knowledge of the resin flow is then essential since it allows to estimate the filling duration or the location of dry areas which are critical for the material [5]. Permeability (i.e. the ability of the medium to be crossed by a liquid) then appears as a key factor in an industrial frame setting [6–9]. This quantity has been introduced by H. Darcy based on experimental observation to link the pressure drop to the flow-rate within porous media in permanent regime [10]. Initially derived from unidirectional flows, Darcy's law has been extended through homogeneisation theory [11]. However, the 1D linearised volumetric flow rate formulation is still widely used to compute permeability [12–14]:

$$\frac{Q}{A} = -\frac{K}{\mu}\frac{\Delta P}{L} \tag{1}$$

where K is the permeability, μ the viscosity of the fluid, Q the volumetric flow rate through a cross sectional area A, ΔP a pressure differential, and L the flow length. Here K refers to a saturated permeability defined when two phases are present in the area of interest: a liquid phase (resin) and a solid phase (reinforcement). When a third gas phase (air) is present, we refer to unsaturated permeability. Since a saturated established flow regime is considered here with only solid and liquid phase (resin and reinforcement), we therefore study saturated permeability further referred to as permeability.

In practice, measuring, modelling and predicting permeability is a real challenge because of the multi-scale nature of the fibrous medium (Fig.1) [15–17]. Indeed, for architectured composites, the resin flow can be observed between yarns, formed of thousands of unidirectional fibres (inter-yarn zone) [9], but also inside them (intra-yarn zone) [16, 18–20] (Fig. 1).

*Corresponding author
Email address: nmoulin@emse.fr (Nicolas Moulin)

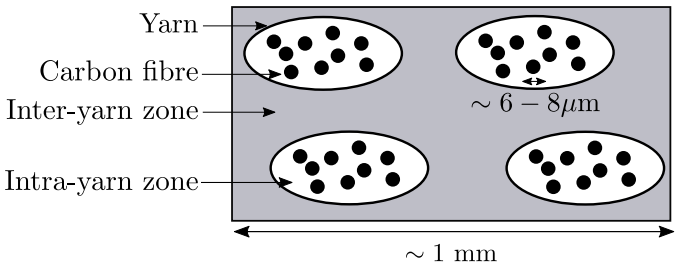

Figure 1: Dual-scale nature of the fibrous medium.

In numerical studies about saturated permeability, the intra-yarn zone is considered as a bundle of fibres where each fibres (at the microscopic scale) is described, or as an impermeable medium, or again as an equivalent Darcy's medium with a very low permeability (at the mesoscopic scale) [5, 21, 22]. Nevertheless, neglecting intra-yarn permeability may be questionable depending on both local fibre volume fraction in the yarns ($V_{f,yarn}$) and overall fibre volume fractions (V_f) [16, 23–25]. A more precise study should therefore be carried out to see up to which value the intra-yarn permeability should be neglected. Despite a significant number of studies on dual-scale permeability of fibrous media [16, 20, 26–28], the numerical computation of permeability remains challenging. Indeed, numerical simulations can be difficult in particular because of the variability and complexy of the fibrous medium (reinforcement geometry) [29], the upscaling procedure [30] and, finally, the coupling between Stokes-Darcy and/or Brinkman's equations [31].

Permeability calculation can also be delicate for complex geometries with high anisotropy such as ply-to-ply interlock fibrous structures. Those geometries have a 3D structure in which a yarn passes through the thickness (*binder yarn*) to bind different layers and thus increase mechanical performances [4, 32]. The presence of complex fibrous architectures is a significant barrier to analytical approaches. Indeed, such models commonly used are usually limited to ideal two-dimensional arrangements [24, 33–35]. However, more complex geometries have also been studied [36, 37] even though it is often required to simplify the internal structure. Broadly speaking, analytical derivation of permeability consists in solving Stokes' equation for a given geometry before making an identification with the Darcy's law. The experimental characterisation of permeability [28, 38–41] is still a challenge due to the variety of experimental procedures using different

measurement systems (existing methods have not yet been standardised). Experiment results show a significant scatter due to the design of the test set-up, fluid pressure and viscosity measurement, textile variations, and data analysis [42–45].

A numerical approach has been used here to address the multi-scale permeability [16, 20] of different fibrous media. Numerical permeability is traditionally calculated by solving the Stokes' equation on a unit cell whose permeability is supposed to be representative of the overall structure [12, 46–48]. Those unit cells can be obtained through textile modelling software such as WiseTex [49–51] or MULTIFIL [52, 53], sample scanning [13] or X-Ray microtomography acquisition (μCT) [1, 47, 54]. In μCT generated models, the image segmentation step is a tricky stage that can lead to underestimation of the solid volume fraction and hence numerical errors in the computation of permeability values [54].

Then, considering permeable yarns, the intra-yarn zone is considered as a Darcy's medium and a coupled Stokes-Darcy flow is then observed. Brinkman's equation [55] is also widely used instead of Darcy's one, using Lattice Boltzmann Method (LBM) [56], Finite Element Method (FEM) [27, 46], asymptotic homogenization technique [57] and, recently, Proper Generalized Technique (PGD) [31] to compute the permeability tensor of wowen fabrics.

Belov et al. [56], for instance, but also Syerko et al. [31] and Tahir et al. [25], have focused on Brinkman's equation that does not allow to investigate very low permeability values for intra-yarn due to numerical issues. It also requires to define a permeability for the inter-yarns channels, which has no physical meaning. Indeed, with this method, Belov et al. [56] expect to obtain an asymptotic value of permeability when intra-yarn permeability decreases, which cannot be reached with their method. The present paper will confirm this hypothesis and describe more accurately the transition using a larger range of intra-yarn permeabilities.

Indeed, the main novelty of our work is to address the dual-scale permeability problem with a Stokes-Darcy monolithic approach rather than solving Brinkman's equation commonly used in literature [25, 31]. This model requires to define an equivalent permeability for inter-yarn spaces. This approach displays two major issues. The first one is the need of a non-physical permeability so as to solve Brinkman's equation in the

inter-yarn areas. The second one is a difficult to solve the problem when the intra-yarn permeability becomes extremely low. The numerical strategy thus requires a high robustness to overcome the huge gap of properties. The Stokes-Darcy monolithic strategy enables to bypass such an issue and to simulate flows with very low values of intra-yarn permeability.

The originality of the approach developed in this paper lies in the description of a continuous description of Stokes (with impervious yarns) - Stokes-Darcy (with permeable yarns) transition for a wide range of intra-yarn permeability without description of an equivalent permeability [25, 31] for inter-yarn spaces. This approach enabled for the first time to validate a semi-analytical model on the entire range of calculation even after reaching the asymptotic value of permeability. This will allow to propose an empirical law to correlate intra-tow permeability to the permeability of the whole fabric. Our work enables to extend formulas initially derived empirically for idealised periodic fibre packings [58, 59] to real materials with complex 3D architectures at the mesoscopic scale.

We used here a mixed velocity-pressure finite element formulation to solve the Stokes-Darcy coupled problem. This formulation has been developed in previous studies [60–64] and implemented in the Z-set software suite [65]. This approach is based on a monolithic strategy [62], consisting in defining one single mesh for discretising the computational domain (Stokes and Darcy domains). The formulation is then stabilised with a Variational Multi-Scale Method (VMS) [66], more specifically the ASGS (Algebraic Sub-Grid Scale) [62, 67] method.

In this paper, after validating the numerical method by comparing the permeability results with analytical values, dual-scale permeability of regular arrangements will be studied. Three-dimensional flow simulations (Stokes and Stokes-Darcy) within interlock ply-to-ply unit cells will be presented. An empirical law to link the effective permeability (i.e. the permeability of the whole unit cell) to the intra-yarn permeability will be proposed.

2. Materials and Methods

The unit cells and boundary conditions used for the 2D and 3D calculations are presented. Terms 2D or 3D will refer to dimensions of the simulations. The 3D simula-

tions are only performed on 3D ply-to-ply angle-interlock woven fabric unit cell. And, it is important to note that no 2D fabric are used, only 2D flows on idealised periodic packings. The numerical strategy is then briefly reminded: the coupled Stokes-Darcy problem is solved by a monolithic mixed velocity-pressure formulation stabilised by an ASGS method.

2.1. Virtual materials

2.1.1. Periodic packings

In order to validate the numerical method and verify the accuracy of the approach, 2D periodic packings have to be described. The aim was, in first approach, to use well known geometries to obtain permeabilities that can be predicted analytically from literature [33, 35]. The two common arrangements of hexagonal and quadratic packing are presented in Fig.2a and Fig.2b respectively.

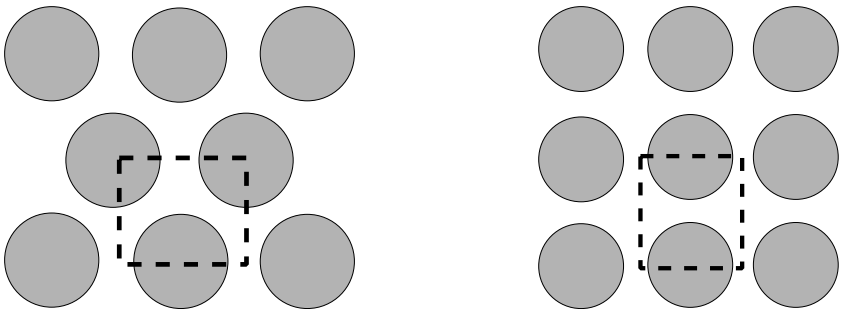

(a) Hexagonal arrangement (b) Quadratic arrangement

Figure 2: Representative cell for hexagonal (a) and quadratic (b) arrangements in dash line (inspired of [35]).

Elementary volume geometries, relative boundary conditions and associated meshes are represented in Fig.3 and Fig.4. In compliance with literature [33, 35], the velocity field is nil on fibres, the normal velocity component is zero on edges, and a pressure gradient is imposed. Simulations have been performed with Z-set software [65] for a Stokes' flow stabilised by ASGS method. The pressure differential applied here is 1 bar for a fluid viscosity μ=10 Pa.s. Though these values may seem high, tests have been carried out to show that neither the value of μ nor ΔP have an influence on the final permeability result after applying the Darcy's law. This can be explained by the absence

of fluid/solid interaction in the present model. The Finite Elements (FE) method used for simulation in Z-set software will be presented in the associated section.

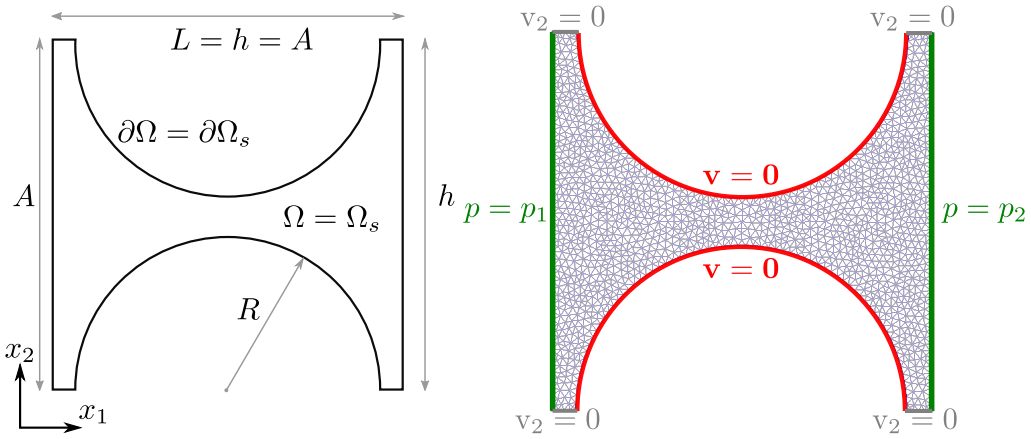

Figure 3: Representative volume geometry for the quadratic arrangement (a) and the corresponding mesh (1,447 nodes / 2,898 linear triangle elements) with associated boundary conditions (b).

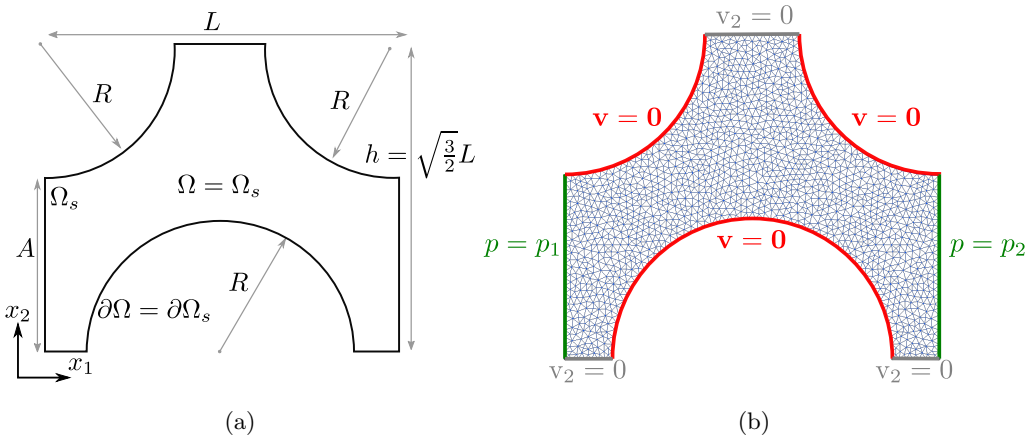

Figure 4: Representative volume geometry for the hexagonal arrangement (a) and the corresponding mesh (1,560 nodes / 3,123 linear triangle elements) with associated boundary conditions (b).

135 The aim is to compare analytical and numerical results for simple arrangements widely studied in literature [33, 35]. We use models initially established at the microscopic scale, with periodic packings of fibres, to validate mesoscopic results with yarns considered as

a regular arrangement of cylinders. Indeed, the derivation of these analytical formulas is not directly based on a specific scale but only relies on the topology of the flow channels. One of the originality of our approach is to validate our model on those well known models and extend it to permeable fibres, that could then be considered as idealised yarns. A special attention have to be paid in this case to the interpretation of the results, in particular because of the definition of a yarn volume fraction and the common fibre volume fraction (see below).

Both configurations are thus studied : hexagonal (Fig.2a) and quadratic (Fig.2b). For those configurations, Gebart [35] used hydrodynamic lubrication approximations and solved the Stokes' equation. By identification with Darcy's law, the normalised transverse permeability K is finally given by:

$$K = \beta \left(\sqrt{\frac{V_{f,max}}{V_f}} - 1 \right)^{\frac{5}{2}} \tag{2}$$

Parameters β and $V_{f,max}$ of Eq.2 are given in Tab.1. As Eq.2 has first been derived for fibre arrangements, V_f normally refers to a fibre volume fraction. Since our study focuses on the mesoscopic scale, it is more thorough to consider V_{yarn} which corresponds to a yarn volume fraction. The yarn volume fraction (V_{yarn}) corresponds to the volume of the yarns divided by the total volume of the unit cell. This quantity can be linked to the common fibre volume fraction V_f with the following relation :

$$V_f = V_{yarn} \cdot V_{f,yarn} \tag{3}$$

where $V_{f,yarn}$ is the ratio of fibres inside the yarns. For example, based on Fig.3 and Fig.4, $V_{yarn} = \pi R^2 / Lh$. This does not alter the validity of Eq.2.

	Quadratic	Hexagonal
β	$\frac{16}{9\sqrt{2}\pi}$	$\frac{16}{9\sqrt{6}\pi}$
$V_{f,max}$	$\frac{\pi}{4}$	$\frac{\pi}{2\sqrt{3}}$

Table 1: Constants related to hexagonal and quadratic arrangements in Gebart's model.

Results will be also compared to Brusckke-Advani's model [33] which can be seen as a synthesis between low fibre fraction analytical models based on cell model [68] and high

fibre fraction ones leaning on hydrodynamic lubrication approximation such as Gebart's model.

2.1.2. 3D model

The 3D ply-to-ply angle-interlock unit cell used in this study has been generated by the fibrous media simulation software MULTIFIL [69]. This FEM software based on an implicit solver allows to determine the initial configuration of entangled material. An enriched kinematical beam model is used in order to take into account the filament transverse deformations.

Initially, MULTIFIL was used to model wire ropes as an assembly of rods undergoing large deformations and submitted to contact-friction interactions [69]. Then twisted yarns composed of elementary fibres or wires and 2D woven fabrics have been also generated and the mechanical response to traction and compression loadings have been studied highlighting the coupling between traction and twisting [70]. Recent studies have been oriented to predict the micro-geometry of a 2D woven [52] or 3D interlock woven [53]. These woven fabrics have been computed at sub-mesoscale by solving the mechanical equilibrium of an assembly of filaments according to the targeted woven pattern. In a recent paper dealing with 3D woven modelling [53], equivalent envelopes of yarns have been reconstructed.

In this study, the fabric model is a 3D woven angle-interlock composed of 27 yarns (12 warp yarns and 15 weft yarns) shared on 6 weft columns and 6 warp planes (Fig.5). This woven modelling was run with 91 filaments per yarn. The whole 3D textile fabric has been thus performed with 2,457 filaments.

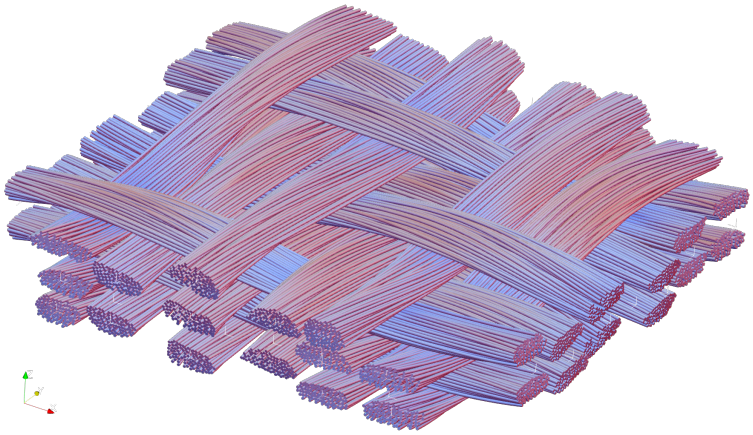

Figure 5: Illustration of the initial configuration of a 3D angle-interlock fabric unit cell at sub-mesoscale.

Then, contours of yarn cross-sections have been computed (Fig.6) from the modelling of the relaxed sub-mesoscale woven pattern in order to reconstruct the mesoscopical model which will be meshed to perform the fluid flow simulations. One of the interesting features which can be captured by calculating tow envelopes is the changes in yarn cross-sections leading to intra-yarn packing factor values. This intra-yarn fibre volume fraction field has been added to show its variability in the woven pattern (Fig.6). The computing reveals that the intra-yarn fibre volume fraction varies on a wide range, from around 50% to 75%. The voxel box edges have been also added (Fig.6). Elements constituting the inter-tow medium have been then deduced from the complementary space between yarns and the edges of the voxel box with dimensions $L_x = 18.73$ mm, $L_y = 18.69$ mm and $L_z = 4.87$ mm.

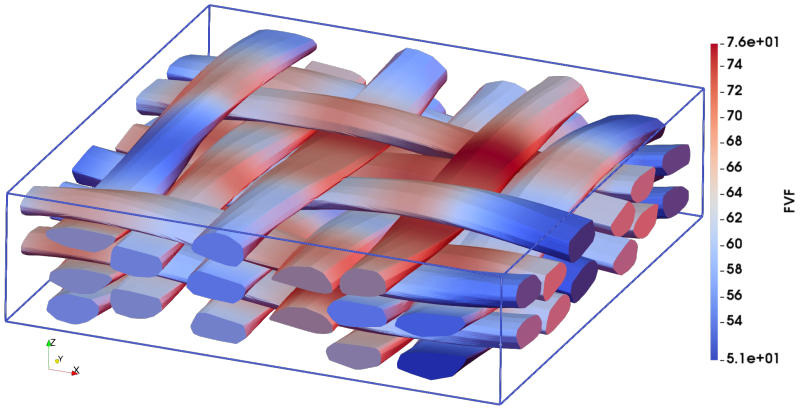

Figure 6: Yarns envelopes from the initial configuration. Superposition of the intra-yarn fibre volume fraction field.

From the meso-geometry of textile fabric, the inter-yarn porous medium has been meshed with linear tetrahedral elements. This unit cell of volume $V = L_x L_y L_z$ is represented in Fig.7. Note that the mesoscopic structure is not periodic.

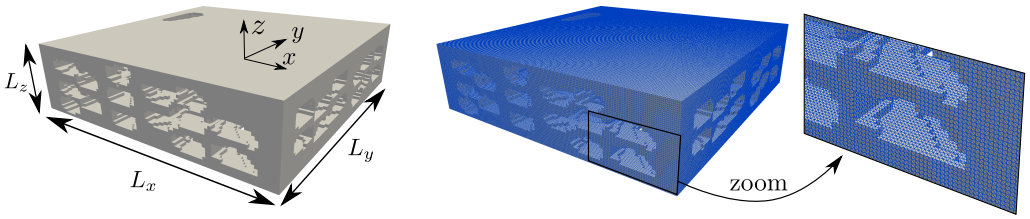

Figure 7: Interlock unit cell and tetrahedral mesh associated ($L_x = 18.73$ mm, $L_y = 18.69$ mm, $L_z = 4.87$ mm) : 135,924 nodes, 581,388 linear tetrahedral elements. Only the resin domain is meshed here (Stokes' flow simulation).

2.2. Numerical strategy

Let Ω be the computation domain, a region of $\mathbb{R}^d$ (with $d = 2, 3$ the spatial dimension) bounded by $\partial\Omega$ (Fig.3a, 4a and 8). The domain Ω represents, at a mesoscopic scale, a specific structure composed of inter-yarn zones if these yarns are considered as impervious (domain Ω_s on Fig.3a or 4a). In the case of permeable yarns, the domain Ω is divided into two non-overlapping sub-domains, Ω_s and Ω_d, separated by a surface $\Gamma = \partial\Omega_s \cap \partial\Omega_d$ (see Fig.8). The problem is to describe the flow of an incompressible Newtonian fluid ruled

by Stokes' equations in Ω_s and by Darcy's equations in Ω_d which represents a porous medium with an intra-yarn permeability K_{intra}. Index s is used to denote everything that concerns the Stokes' domain while index d stands for the Darcy's domain characteristics.

Effects of inertia are neglected, then the motion of the fluid in inter-yarn zones Ω_s is governed by Stokes' equations (momentum and mass conservation):

$$\begin{aligned} -\boldsymbol{\nabla} \cdot (2\mu\dot{\boldsymbol{\epsilon}}(\mathbf{v}_s)) + \boldsymbol{\nabla} p_s &= 0 \quad \text{in} \quad \Omega_s \\ \boldsymbol{\nabla} \cdot \mathbf{v}_s &= 0 \quad \text{in} \quad \Omega_s \end{aligned} \tag{4}$$

where $\dot{\boldsymbol{\epsilon}}$ is the strain rate tensor defined by $\dot{\boldsymbol{\epsilon}}(\mathbf{v}_s) = \frac{1}{2}(\boldsymbol{\nabla}\mathbf{v}_s + \boldsymbol{\nabla}^\top \mathbf{v}_s)$ and μ is the fluid viscosity of the incompressible Newtonian fluid which is assumed to be constant. The vector field $\mathbf{v}_s$ and scalar field p_s are, respectively, the fluid velocity and pressure while $\boldsymbol{\nabla}$ and $\boldsymbol{\nabla}\cdot$ are the gradient and the divergence operators with respect to space coordinates.

The flow of an incompressible fluid through the porous medium Ω_d described by Darcy's equations is given by:

$$\begin{aligned} \mu \mathbf{K}^{-1} \mathbf{v}_d + \boldsymbol{\nabla} p_d &= 0 \quad \text{in} \quad \Omega_d \\ \boldsymbol{\nabla} \cdot \mathbf{v}_d &= 0 \quad \text{in} \quad \Omega_d \end{aligned} \tag{5}$$

where $\mathbf{K}$ is a saturated permeability tensor which can be reduced to a scalar K in an isotropic case, $\mathbf{v}_d$ and p_d the velocity and pressure fields (Darcy's velocity and pressure).

Stokes' and Darcy's equations (Eq.4 and 5) are completed with Dirichlet (denoted D) and Neumann (denoted N) boundary conditions on $\Gamma = \partial\Omega_s \cap \partial\Omega_d$ with $\Gamma_{s,D} \cap \Gamma_{s,N} = \varnothing$ and $\Gamma_{d,D} \cap \Gamma_{d,N} = \varnothing$:

$$\begin{aligned} \mathbf{v}_s &= \mathbf{v}_0 \quad \text{on} \quad \Gamma_{s,D} & \qquad \mathbf{v}_d \cdot \mathbf{n}_d &= v_0 \quad \text{on} \quad \Gamma_{d,D} \\ \boldsymbol{\sigma}_n &= -p_{e,s}\mathbf{n}_s \quad \text{on} \quad \Gamma_{s,N} & \qquad p_d &= p_{e,d} \quad \text{on} \quad \Gamma_{d,N} \end{aligned} \tag{6}$$

where $\mathbf{n} = \mathbf{n}_s = -\mathbf{n}_d$ is the outward unit vector normal to the interface Γ. $\mathbf{v}_0$ and v_0 are, respectively, the velocity prescribed on the boundary $\Gamma_{s,D}$ and $\Gamma_{d,D}$, $\boldsymbol{\sigma}_n$ the normal stress prescribed on $\Gamma_{s,N}$ and $p_{e,\cdot}$ a pressure prescribed on $\Gamma_{\cdot,N}$.

A special attention is paid to the specific conditions on the interface separating Stokes' and Darcy's domains (the interface at the yarn surface). Three conditions are to be prescribed on this interface Γ (Fig.8): the mass conservation, the continuity of the normal stress through the interface, and the Beavers-Joseph-Saffman (BJS) condition [71] allowing to control the tangential component of the velocity on the interface. Considering the

very low permeability values in the yarn (down to 10^{-15} m^2) and the numerical methods implemented in this study for the Stokes-Darcy coupling, this last boundary condition has no significant influence on the flow [62, 64]. It will therefore not be considered in the following of this work.

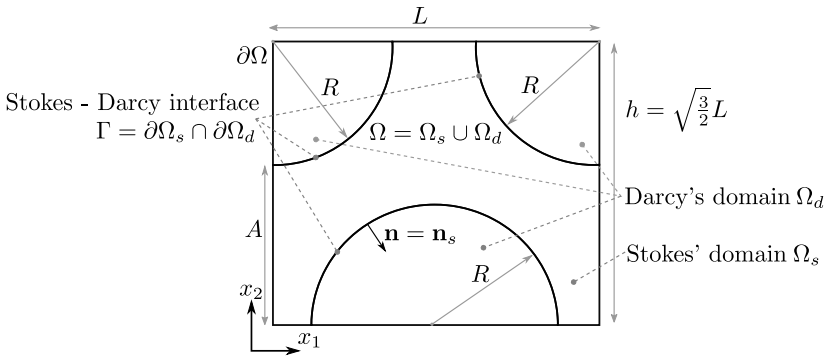

Figure 8: Representative volume geometry for the hexagonal arrangement in the case of permeable yarns considered as Darcy's domains.

Different numerical strategies can be addressed for solving the Stokes-Darcy coupled problem such as the partitioned procedure (a.k.a. decoupled approach) [72, 73] or the monolithic approach (a.k.a. unified approach) [62, 64, 67]. Contrary to partitioned methods, the monolithic approach of the Stokes-Darcy coupled problem consists in using one single non-necessarily structured mesh and the same finite element spaces in Stokes' and Darcy's domains.

A mixed finite element formulation in velocity and pressure is used in the whole domain for Stokes' and Darcy's areas. The weak formulation of the Stokes-Darcy coupled problem is obtained by adding both Stokes' and Darcy's weak formulations and by taking into account the interface conditions described above. Details concerning weak formulations of Stokes, Darcy and coupled Stokes-Darcy systems as well as mathematical functional spaces for solutions and test functions are given in previous studies [60–62].

The computational domain $\Omega \subset \mathbb{R}^d$ is discretized into n_{el} non-overlapping elements $\mathcal{K}$. This one single unstructured mesh is made up of triangles if superscript $d = 2$ (Fig.10) and of tetrahedrons if $d = 3$ (Fig.16). Velocity $\mathbf{v}$ and pressure p are both approximated by continuous and piecewise linear functions (P1/P1 approximation). However, such an

approximation is not stable [62, 67]. This issue is overcome by using a Variational Multi-Scale (VMS) technique [66] in particular the Algebraic Sub-Grid Scale (ASGS) technique [62, 67] consisting in adding some stabilization terms to the Galerkin formulation.

3. Results

The results from Stokes' (impermeable yarns) and Stokes-Darcy flow simulations (permeable yarns) are presented for 2D and 3D geometries. The hypothesis that the yarns can be considered as permeable is then discussed and an empirical law is finally proposed to relate the cell effective permeability to the yarn one.

3.1. 2D flows

3.1.1. Impermeable yarns

The validity of the numerical method is first verified through permeability derivation for ideal tow arrangements widely studied in the literature. Tows are first considered as impermeable: Stokes' flow simulations are thus performed. We therefore rely on quadratic (Fig.2b) and hexagonal (Fig.2a) arrangements for which analytical formulae for transverse permeability can be found in [33, 35]. The numerical permeability has been calculated from the simulations using Darcy's law expressed in flow-rate (Eq.1): a pressure differential is applied on opposite sides and the fluid velocity is zero on the yarns (Fig.3b and 4b). Fig. 9 shows the normalised permeability change for an hexagonal arrangement as a function of V_f (in Gebart's and Bruschke-Advani's models) equivalent to V_{yarn} in our computations. A very good agreement is thus found between the numerical results and the analytical results from the Gebart's [35] and Bruschke-Advani's [33] models (Fig.9). Similar comparisons were also carried out by Nabovati et al. [59] and Tahir et al. [25] but using different numerical methods, the Lattice Boltzmann Method and the Finite Volume Approach respectively.

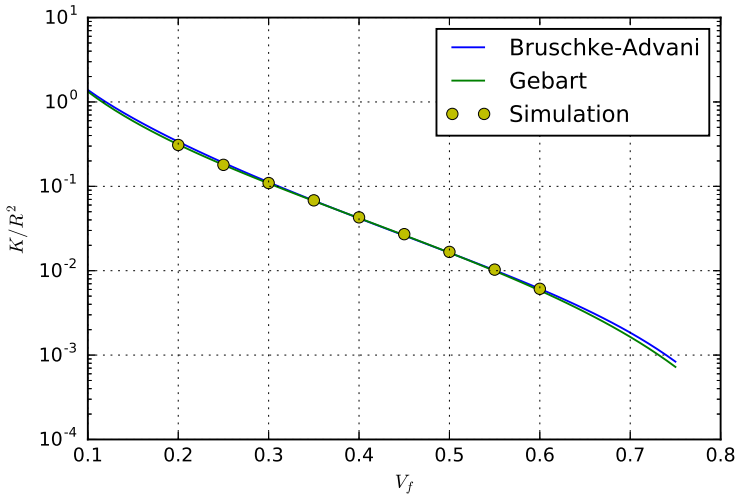

Figure 9: Normalised permeability for a hexagonal arrangement as a function of V_f (equivalent to V_{yarn} in this particular case - Bruschke-Advani's model and Gebart's model simulations).

3.1.2. Permeable yarns

From the same geometries, yarns are now considered as isotropic permeable media modelled by an equivalent homogeneous Darcy's medium (Fig. 8 and 10). A Stokes-Darcy flow is thus achieved by imposing a pressure differential on opposite sides. The intra-yarn permeability K_{intra} (i.e. permeability of Darcy's zones) is an input parameter of the simulation. We call *effective permeability* K_{eff}, the permeability of the whole unit cell. It is derived from the inflow on the overall volume (Stokes' and Darcy's media), and therefore a function of K_{intra}. One can plot the effective permeability as a function of the intra-yarn permeability K_{intra} for given yarn fractions V_{yarn} (Fig.11).

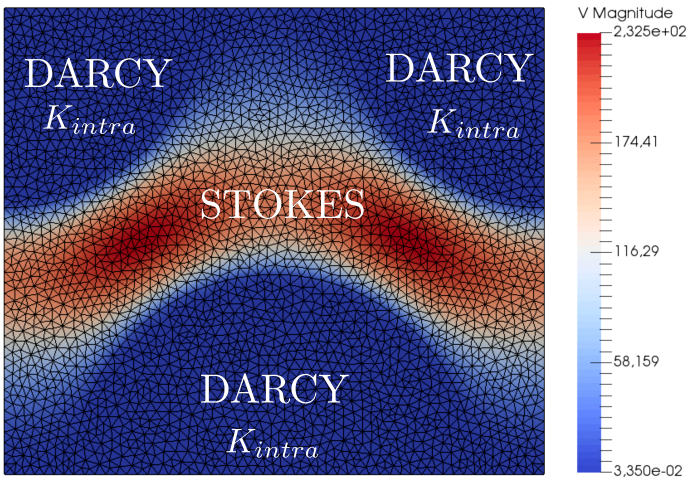

Figure 10: Stokes-Darcy flow within a hexagonal cell unit ($K_{intra} = 10^{-10}m^2$, $\Delta P = 1bar$, $\mu = 10Pa.s$, $V_{yarn} = 0.51$).

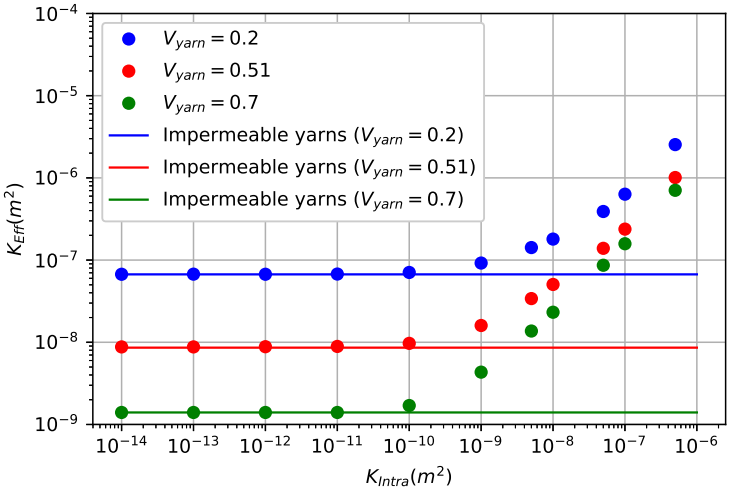

Figure 11: Effective permeability as a function of intra-yarn permeability K_{intra} for different yarn volume fraction V_{yarn}.

The effective permeability tends towards an asymptotic value K_{asympt} for decreasing values of K_{intra}. As expected, this limit corresponds to the values obtained for impermeable yarns, for example K_{asympt} for $V_{yarn} = 0.51$ on Fig.11 (continuous line). Results

of Fig.11 confirm previous models [16, 20, 56] which tend to show that yarn permeability can be taken as null when it is about two orders of magnitude lower than the overall permeability of the fabric. The asymptotic values were compared to the values of the Bruschke-Advani model (Tab.2). The presence of an intra-yarn permeability threshold from which it is reasonable to consider the yarns as impermeable is also highlighted here. We denote as K^{90}_{intra}, the intra-yarn permeability value from which the effective permeability reaches 90% of its asymptotic value. Due to uncertainty on the results, intervals for K^{90}_{intra} are presented in Tab.2. These results are comparable to those described in the literature [28]. The interval K^{90}_{intra} in Tab.2 frames the threshold value proposed by Bodaghi et al. [28] from which the effective permeability is independent of the intra-yarn one.

In average, for V_{yarn} values varying between 0.2 and 0.7, from $K_{intra} = 5 \times 10^{-11}\, m^2$, lowering intra-yarn permeability leads to variations of less than 10% of the asymptotic permeability. In [20] a higher value of this intra-yarn permeability threshold is given (i.e. $K_{intra} \simeq 1 \times 10^{-9}\, m^2$). Identifying this threshold value has important consequences since it can justify the passage from time-consuming Stokes-Darcy simulations to more classical Stokes flows. Taking values presented in [21, 74, 75] as a reference, intra-yarn permeability can reach $10^{-13}\, m^2$ to $10^{-15}\, m^2$. Considering these values, our study may justify the hypothesis that the yarns can be considered as impermeable for a saturated flow in these conditions.

V_{yarn}	K_{asympt} (m^2)	K_{BA} (m^2)	K^{90}_{Intra} (m^2)
0.2	6.72×10^{-8}	7.47×10^{-8}	$[1 \times 10^{-10}, 5 \times 10^{-10}]$
0.51	8.78×10^{-9}	8.60×10^{-9}	$[1 \times 10^{-10}, 5 \times 10^{-10}]$
0.7	1.40×10^{-9}	1.40×10^{-9}	$[1 \times 10^{-11}, 5 \times 10^{-11}]$

Table 2: Asymptotic permeability K_{asympt} from Fig.11, analytical permeability K_{BA} from Bruscke-Advani's model and K^{90}_{Intra} for different V_{yarn}.

At last, an empirical formula may be proposed to link the intra-yarn and the asymptotic permeability to the effective one. By asymptotic reasoning, the following power-law

can be proposed:

$$K_{eff} = K_{asympt}\left[1 + \alpha\left(\frac{K_{intra}}{R^2}\right)^n\right] \tag{7}$$

$$\Leftrightarrow \log\left(\frac{K_{eff}}{K_{asympt}} - 1\right) = \log(\alpha) + n\log\left(\frac{K_{intra}}{R^2}\right) \tag{8}$$

where α and n are two dimensionless constants to be determined and R is the circular yarn radius.

To confirm this expression, linear regressions were plotted according to Eq.8 (Fig.12). The obtained squared correlation coefficients r are superior to 0.999. For a considered arrangement, lines seem to be parallel showing that n may not depend on V_f but should be considered as a function of the configuration. Considering this, the obtained values for n are 0.94 for a quadratic arrangement and 0.82 for a hexagonal arrangement. Coefficient α has to be considered as a function of V_{yarn} and of the arrangement. Further studies should be done to link explicitly n and α to the geometrical parameters and to give them a physical meaning.

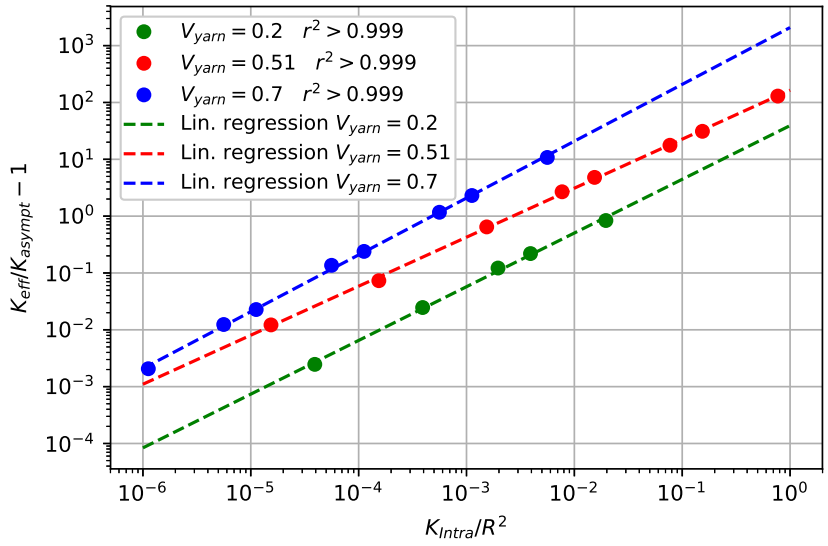

Figure 12: $K_{eff}/K_{asympt} - 1$ (log scale) as a function of K_{intra}/R^2 (log scale) for different V_{yarn} (quadratic arrangement) and linear regressions.

In [27] a Stokes-Brinkman coupled flow is simulated to compute the effective perme-

ability of unit cells for simple tow arrangements. Based on theoretical arguments, an analytic formula is also proposed for a hexagonal arrangement of ellipsoidal fibre yarns when $\sqrt{K_{intra}/R^2} \gg K_{intra}/R^2$:

$$K_{eff} = C_1 + C_2\sqrt{K_{intra}} \tag{9}$$

where C_1, C_2 are constants determined by data fitting. It seems interesting to notice that Eq.7 and Eq.9 have a roughly similar form. However, in Eq.7, the value $n = 0.5$ is not found.

A similar formula can be found in literature [20, 58]. Permeability of hexagonal and quadratic arrangements with permeable yarns is studied analytically through a Stokes-Darcy coupled problem. The transverse permeability is given by:

$$K_{eff} = K_{asympt} + K_{intra} + C_{Shou}H_{min}\sqrt{K_{intra}} \tag{10}$$

where C_{Shou} is a coefficient and H_{min} the minimal distance between tows depending on the packing (Tab.3). Numerical values from Shou's model [20] and the present empirical power-law have been compared in Fig.13. The coefficient C_{Shou} has been determined by data fitting: for the hexagonal arrangement $C_{Shou} = 1.33$ and for the quadratic arrangement $C_{Shou} = 0.63$. The constants α and n are obtained through previous linear regressions. One can observe that both models coincide for low K_{intra} values. For higher values, the power-law model seems to be more pertinent. However for RTM modelling, intra-yarn permeabilities usually have very low values [74, 75], therefore both expressions can be used for effective permeability predictions. Theoretical studies should then be done to justify Eq.7 even if it shows an excellent agreement with numerical results.

	Quadratic	Hexagonal
H_{min}	$R\left(\sqrt{\frac{\pi}{V_{yarn}}} - 2\right)$	$R\left(\sqrt{\frac{\sqrt{3}\pi}{2V_{yarn}}} - 2\right)$

Table 3: Minimal distance between yarns for quadratic and hexagonal arrangements.

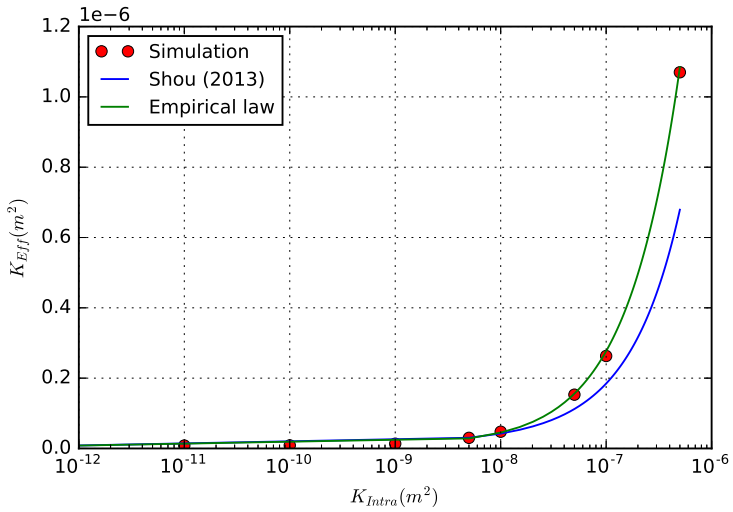

Figure 13: Comparison between Shou's model and the empirical power-law (quadratic arrangement, $V_f = 0.51$).

3.2. 3D flows

3.2.1. Impermeable yarns

After previous validations in 2D, flows were then simulated inside a 3D ply-to-ply interlock unit cell provided by Safran Aircraft Engines (Fig.7). Stokes flow simulations have been first performed (Fig.14, Fig.15). The simulations on the finest mesh ($\sim 10^6$ nodes) run in less than an hour using the direct solver MUMPS [76] used in Z-set software [65]. So as to derive permeability in direction i ($i = x, y, z$), a pressure differential $\Delta P = 10^5$ Pa is imposed on the faces perpendicular to i axis. As regards the velocity field, it is taken as nil on the yarns and the normal component is zero on the other boundaries. The permeability is then computed through flow-rate formulation of Darcy's law.

For instance, in x direction:

$$K_{xx} = \frac{\mu L_x Q}{L_y L_z \Delta P} = \frac{\mu L_x}{L_y L_z \Delta P} \int_{y=0}^{y=L_y} \int_{z=0}^{z=L_z} v_x(y,z)\, dydz \tag{11}$$

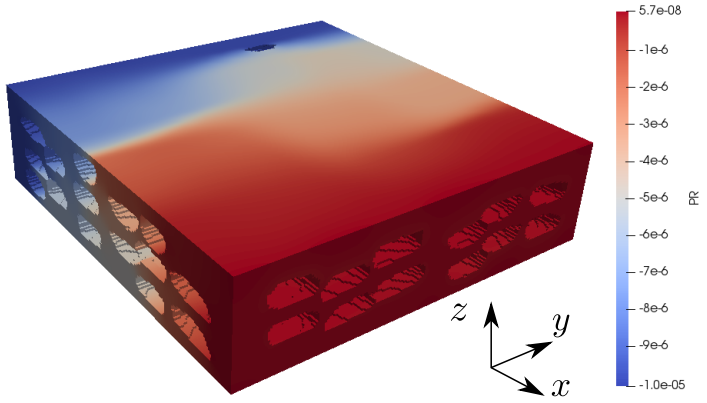

Figure 14: Pressure field (MPa) for a pressure gradient along x axis.

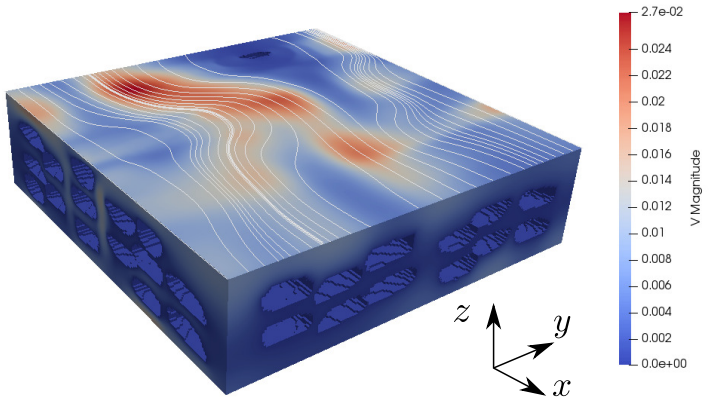

Figure 15: Magnitude of velocity field (mm.s^{-1}) with streamlines (white lines) on the top of the cell for a pressure gradient along x axis.

Several assumptions had to be made here. First, we assumed that the flow-rate formulation of Darcy's law holds for flows in highly anisotropic environments. In addition, we considered the warp/weft/transverse directions as the principal directions, which may be questionable. This assumption has however been justified by computing the principal directions from 3D formulation of Darcy's law.

Permeability, considered as a diagonal tensor since the principal directions are supposed, in first approach, to be aligned with the fabric main directions, is then computed (Tab.4). The transverse permeability K_{zz} is lower than the others, as expected. One

should notice that the values are surprisingly high compared to literature at similar fibre volume fraction [36, 77]. However, this might be explained by the relatively low value of V_{yarn} ($V_{yarn} = 0.56$): the fluid can easily go through the preform. Assuming that inside the yarns, the fibres are hexagonally arranged at the theoretical maximum compaction, we obtain that the overall fibre volume fraction is $V_f = 0.51$, which is a relatively low value for a structural composite.

K_{xx} (m^2)	K_{yy} (m^2)	K_{zz} (m^2)
3.27×10^{-8}	5.29×10^{-8}	1.24×10^{-8}

Table 4: Numerical permeability in the three directions for the unit cell presented in Fig.7.

3.2.2. Permeable yarns

Stokes-Darcy flows within the interlock unit cell have also been studied. Yarns are now considered as isotropic permeable media of a given permeability K_{intra}. A pressure drop is applied again on opposite edges of the whole volume. Stokes-Darcy flows are thus obtained (Fig.16). Effective permeability K_{eff} as a function of the intra-yarn permeability K_{intra} has been plotted in Fig.17.

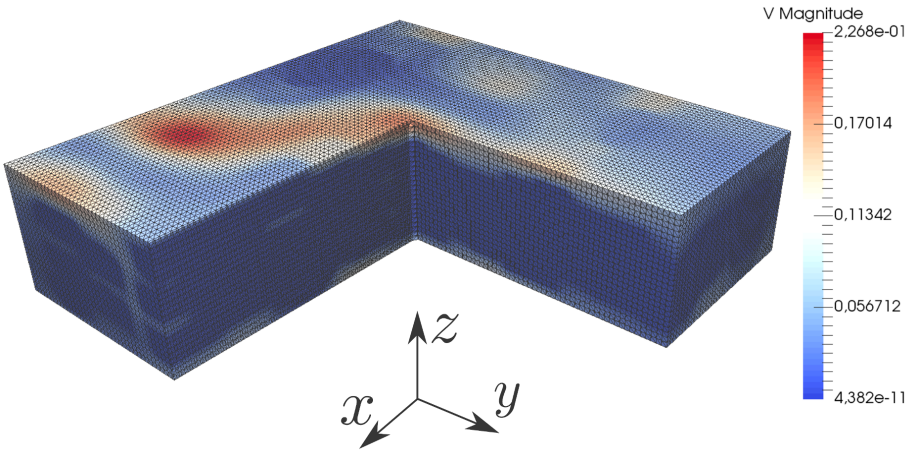

Figure 16: Cross-section of a Stokes-Darcy flow within the interlock unit cell (velocity magnitude, mm/s, $K_{intra} = 5 \times 10^{-8}$ m^2).

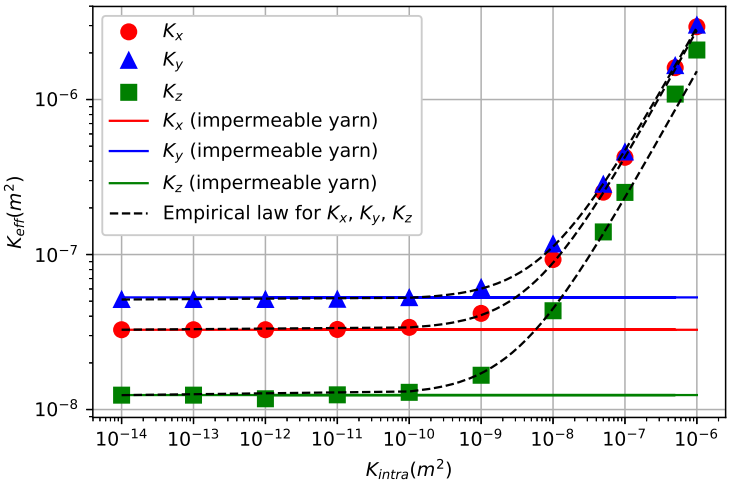

Figure 17: Effective permeability as a function of the intra-yarn permeability: numerical results and empirical law. Results are compared to those obtained for impermeable yarns (Stokes' flow simulation).

On Fig. 17, we observe again that the effective permeability tends towards permeability obtained for impermeable yarns when intra-yarn permeability decreases. The validity of the empirical law proposed has been tested again, for which yarn geometrical characteristics is now included in a new coefficient α':

$$K_{eff} = K_{asympt}\,(1 + \alpha' K_{intra}^{n}) \tag{12}$$

where α' and n are two constants to determine.

An excellent agreement between Eq.12 and numerical results can be noticed (Fig. 17). In this case again, the coefficient n can be considered as constant and $n = 0.84$. We have here in average $K_{intra}^{90} \sim 5 \times 10^{-10}$ m^2. Referring ourselves to intra-yarn permeability results from [21, 74, 75], yarns may be considered as impermeable in our case.

Regarding this intra-yarn permeability threshold in general, one may consider that microscopic effects (i.e. linked to the internal yarn structure) become negligible when the intra-yarn permeability is much lower than permeability with impermeable yarns. From the 2D and 3D results presented before, we observe: $K_{intra}^{90} \sim 100 \cdot K_{asympt}$ which corresponds to an upper bound value considering the literature values summed up in [28]. This result should depend on fibre orientation, intra-yarn permeability anisotropy, or the

value of V_{yarn}.

4. Discussion

4.1. Unit cell definition for permeability computation

Relatively high permeability values are mainly due to the phenomenon of race-tracking. Indeed, dominant flows or preferential flow channels are observed, mainly on the surface, which means that the fluid mainly flows along these paths (Fig.15 and Fig.18). The surface contribution (preferential flows) is then significant: up to one or two orders of magnitude higher than the one within the preform. This phenomenon is explained in particular by geometrical issues: surface channels, resulting from the generation of volume, are much wider than the internal architecture of the material [37]. Therefore, these are channels that offer less resistance across the volume. In the end, the numerical permeability can be overestimated. This observation therefore leads to question the representativeness of the volume considered, especially if those volumes are not periodic. Two methods have been compared to limit the impact of preferential flows: the reduction of calculation area during post-processing and mesh clippings.

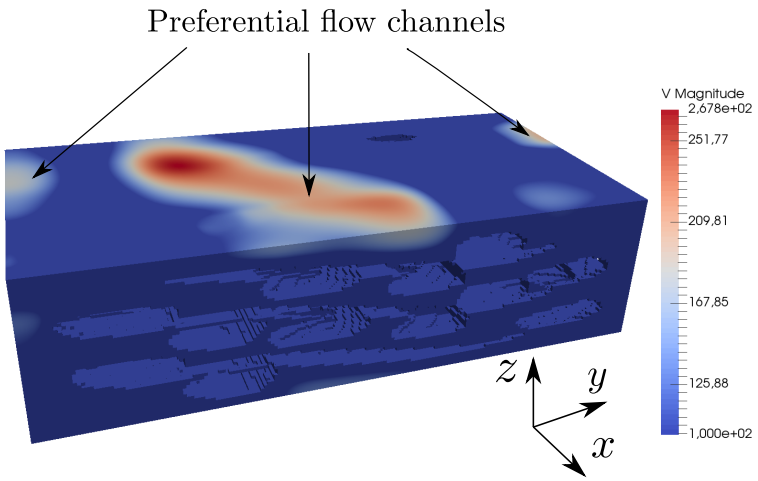

Figure 18: Highlighting preferential flow channels within the preform ($\Delta P = 1$ bar, pressure gradient along x-axis). The picture has been rescaled: the velocity magnitude lower than $100\,mm.s^{-1}$ is depicted in dark blue.

4.2. Reducing the impact of preferential flows

Permeabilities have been calculated by reducing the area on which the flow is calculated (*calculation area*) during post-processing. The initial mesh on which the simulation is performed is unchanged. By reducing the calculation area (Fig.19), it is possible to limit the preferential flow contribution. The geometrical centre of the different surfaces remains the same. Reduction of calculation area in the three directions is presented in Fig.20. For transverse flow, permeability converges towards a consistent value. This convergence may be explained by the fact that other preferential flow channels are present in the transverse direction especially in the interstitial areas between warp and weft yarns. For the other two directions, no convergence is observed. Reducing calculation area leads to a loss of information: the computed flow-rate decreases without converging.

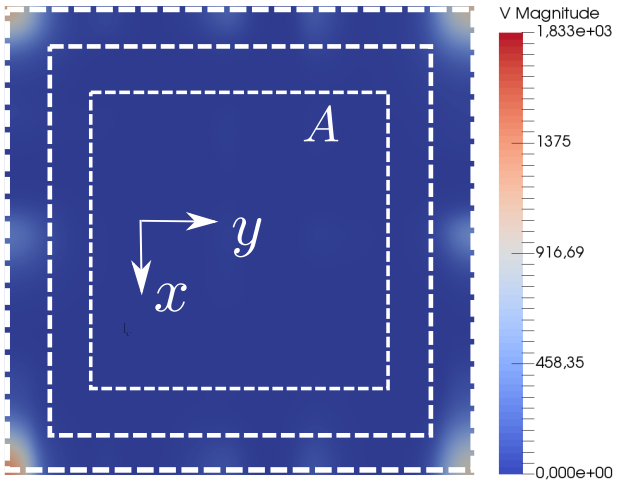

Figure 19: The calculation area is reduced (transverse flow here): the initial area is A_0. The geometrical centre is the same for the different calculation surfaces.

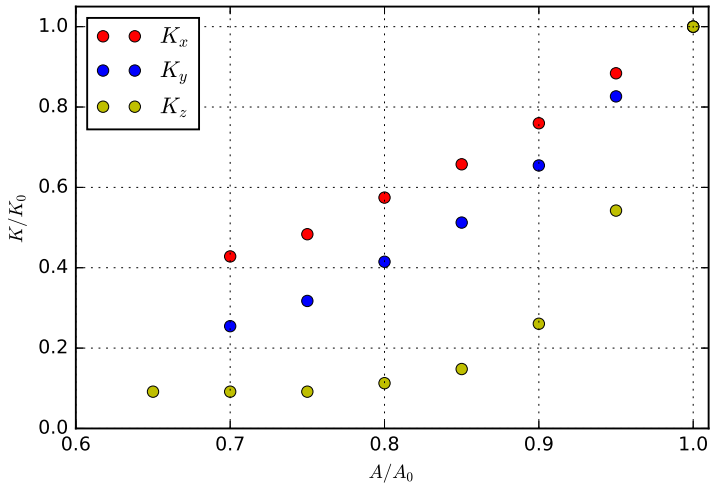

Figure 20: Normalised permeability K/K_0 as a function of normalised calculation area A/A_0. The zero subscript refers to the initial area (i.e. maximal area). The geometrical centre of the calculation area remains the same.

Another solution is to directly reduce mesh sizes by removing external layers of elements. This also reduces the importance of preferential flows. Successive outer layers of elements have been removed: permeability is then calculated from flows simulated in reduced volumes. First, edges perpendicular to the x and y axes have been cut while leaving the edges perpendicular to the z axis unchanged. The results of *transverse* permeabilities were compared to those obtained by reducing the calculation area (Fig.21). In all the mesh cuts presented, the geometrical centre of the volume remains the same. Both methods (computation area reduction and mesh clipping methods) are not strictly equivalent since the asymptotic values differ. In both cases, it would seem necessary to reduce the surface area by at least 20% to avoid preferential flows. One of the limits of mesh redrawing lies in the fact that beyond a certain level of division, one can lose mesh connectivity. This causes considerable problems for the numerical resolution of the system. In addition, cut planes coincide with voxel rows meaning that a sufficiently fine mesh is required.

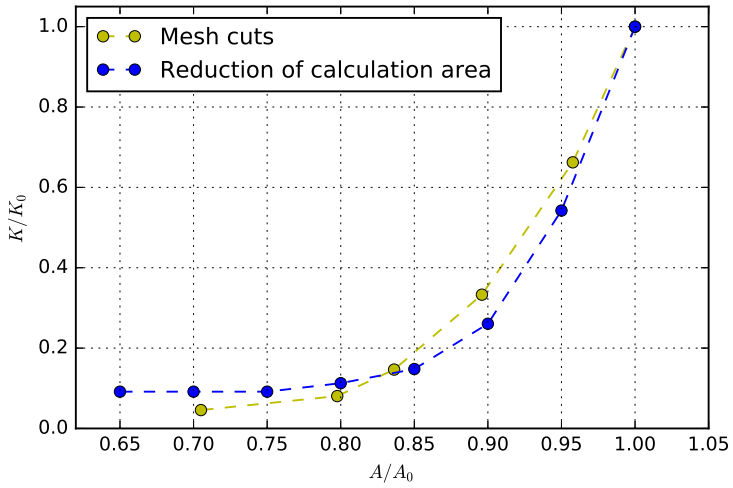

Figure 21: Normalised transverse permeability as a function of normalised surface : comparison between mesh cuts and reduction of the calculation area during post-processing. Data have been normalised by the values obtained for the initial area (A_0,K_0).

5. Conclusion

We have here studied the numerical permeability of 2D and 3D geometries from a monolithic finite element approach implemented in Z-set software suite. Two dimensional transverse flows have first been carried out for simple regular arrangements. For impermeable yarns, Stokes' flows have been simulated leading to numerical permeabilities in excellent agreement with analytical results from Gebart's and Bruschke-Advani's models on quadratic and hexagonal packings. This allowed to justify the validity of the numerical approach. Yarns have been then considered as permeable. Stokes-Darcy flow simulations have thus been performed for given values of intra-yarn permeability. We observed that the effective permeability tends towards permeability calculated from Stokes simulations when intra-yarn permeability becomes increasingly lower. Convergence of effective permeability to an asymptotic permeability have been described from computations on a large range of K_{intra}. The main novelty of this paper lies in the continuous description of transition from Stokes-Darcy (permeable yarns) to Stokes flows (impervious yarns), for both ideal packings and realistic 3D structures. In compliance with literature, this

highlights the presence of an intra-yarn permeability threshold from which the yarns can be considered as impermeable so that Stokes' simulations are sufficient to give consistent results.

The same approach has then been applied for 3D ply-to-ply interlock. Stokes' flows, in other words flows with impervious yarns, lead to uncommonly high values of permeabilities which can be explained by the phenomenon of preferential flows. In order to limit the influence of edge flows, two methods have been proposed: reducing the calculation area during post-processing and cutting the edges of the mesh. However, neither of both have really been conclusive and more thorough works should be done to suggest a more efficient way to diminish those effects. This problem is major since it has a great influence on numerical permeability values and questions the representativeness of the unit cell for permeable and impermeable yarns, and should be the main focus of further studies. The empirical law which links the effective permeability and the intra-yarn one seems to be valid for both 2D and 3D flows. Such a law may be used in practice as a reverse method to estimate intra-yarn permeability from the effective one. At last, threshold values can also been noticed from which one can simply use Stokes' simulations instead of Stokes-Darcy ones. As for the two-dimensional cases, these threshold are superior to realistic values of intra-yarn permeability. As a consequence, this work defines the limits of the hypothesis according to which yarns can be considered as impermeable for saturated flows. This is an important result as it enables to simplify greatly the simulations and to make them significantly. Further works will focus on an accurate definition of the non-uniform local volume fraction $V_{f,yarn}$ in order to evaluate the effect of a non-constant intra-yarn permeability K_{intra} on effective global permeability. The ultimate goal will be to study both experimentally and numerically the impregnation of 3D-interlocks including weeting [78–80] and capillary [81, 82] effects.

References

[1] M. A. Ali, R. Umer, K. A. Khan, S. Bickerton, W. Cantwell, Non-destructive evaluation of through-thickness permeability in 3d woven fabrics for composite fan blade applications, Aerospace Science and Technology (82-83) (2018) 520–533.

[2] B. Martin, S. Comas-Cardona, C. Binetruy, N. Billon, J. L. Bouvard, P. Lucas, Influence of fabrics design parameters on the morphology and 3d permeability tensor of quasi-unidirectional non-crimp fabrics, Composites Part A: Applied Science and Manufacturing 90 (2016) 470–479.

[3] V. Michaud, A. Mortensen, Infiltration processing of fibre reinforced composites:governing phenomena, Composites: Part A 32 (2001) 981–996.

[4] N. Vernet, F. Trochu, Analysis and modeling of 3d interlock fabric compaction behavior, Composites Part A: Applied Science and Manufacturing 80 (2016) 182–193.

[5] M. Bodaghi, A. Vanaerschot, S. Lomov, N. Correia, On the variability of mesoscale permeability of a 2/2 twill carbon fabric induced by variability of the internal geometry, Composites Part A Applied Science and Manufacturing 101 (01) (2017) 394–407.

[6] H. Alhussein, R. Umer, S. Rao, E. E. Swery, S. Bickerton, W. Cantwell, Characterization of 3d woven reinforcements for liquid composite molding processes, Journal of Materials Science 51 (6) (2016) 3277–3288.

[7] C. Demaria, E. Ruiz, F. Trochu, In-plane anisotropic permeability characterization of deformed woven fabrics by unidirectional injection. part i: Experimental results, Polymer composites 28 (6) (2007) 797–811.

[8] P. J. Liotier, Q. Govignon, E. Swery, S. Drapier, S. Bickerton, Characterisation of woven flax fibres reinforcements: Effect of the shear on the in-plane permeability, Journal of Composite Materials 49 (27) (2015) 3415–3430.

[9] E. E. Swery, T. Allen, P. Kelly, Capturing the influence of geometric variations on permeability using a numerical permeability prediction tool, Journal of Reinforced Plastics and Composites 35 (24) (2016) 18021813.

[10] H. Darcy, Les fontaines publiques de la ville de dijon, Dalmont.

[11] S. Whitaker, Flow in porous media i: A theoretical derivation of darcy's law, Transport in porous media 1 (1) (1986) 3–25.

[12] L. Fang, J. Jiang, J. Wang, C. Deng, The effect of nesting on the inplane permeability of unidirectional fabrics in resin transfer molding, Polymer Composites 37 (6) (2014) 1695–1704.

[13] E. E. Swery, R. Meier, S. Lomov, K. Drechsler, P. Kelly, Predicting permeability based on flow simulations and textile modelling techniques: Comparison with experimental values and verification of flowtex solver using ansys cfx, Journal of Composite Materials 50 (5) (2016) 601615.

[14] D. Woerdeman, F. P. Jr, R. Parnas, Interpretation of 3-d permeability measurements for rtm modeling, Polymer Composites 16 (6) (1995) 470–480.

[15] M. Nordlund, T. Lundström, Effect of multi-scale porosity in local permeability modelling of non-crimp fabrics, Transport in Porous Media 1 (73) (2008) 109–124.

[16] T. D. Papathanasiou, On the effective permeability of square arrays of permeable fiber tows, International Journal of Multiphase Flow 23 (1) (1997) 81–92.

[17] F. Zhou, N. Kuentzer, P. Simacek, S. Advani, S. Walsh, Analytic characterization of the permeability of dual-scale fibrous porous media, Composites Science and Technology 66 (15) (2006) 2795–2803.

[18] L. Chevalier, J. Bruchon, N. Moulin, P.-J. Liotier, S. Drapier, Accounting for local capillary effects

in two-phase flows with relaxed surface tension formulation in enriched finite elements, Comptes Rendus Mcanique 346 (8) (2018) 617–633.

[19] Y. Liu, N. Moulin, J. Bruchon, P.-J. Liotier, S. Drapier, Towards void formation and permeability predictions in LCM processes: A computational bifluidsolid mechanics framework dealing with capillarity and wetting issues, Comptes Rendus Mcanique 344 (45) (2016) 236–250.

[20] D. Shou, L. Ye, Y. Tang, J. Fan, F. Ding, Transverse permeability determination of dual-scale fibrous materials, International Journal of Heat and Mass Transfer 58 (1-2) (2013) 532–539.

[21] C. Li, A. Cantarel, X. Gong, Influence of structural parameters at microscale on the fiber reinforcement, Journal of Composite Materials 53 (7) (2019) 863–872.

[22] B. Yu, L. J. Lee, A simplified in-plane permeability model for textile fabrics, Polymer Composites 21 (5) (2000) 660–685.

[23] L. Silva, G. Puaux, M. Vincent, P. Laure, A Monolithic Finite Element Approach to Compute Permeabilityatc Microscopic Scales in LCM Processes, International Journal of Material Forming 3 (S1) (2010) 619–622.

[24] T. A. K. Sadiq, S. G. Advani, R. S. Parnas, Experimental investigation of transverse flow through aligned cylinders, International Journal of Multiphase Flow 21 (5) (1997) 755–774.

[25] Tahir, M. W. and Hallström, S. and Akermo, M., Effect of dual scale porosity on the overall permeability of fibrous structures, Composites Science and Technology 103 (2014) 56 – 62.

[26] N. Kuentzer, P. Simacek, S. G. Advani, S. Walsh, Permeability characterization of dual scale fibrous porous media, Composites Part A: Applied Science and Manufacturing 37 (11) (2006) 2057 – 2068.

[27] W. R. Hwang, S. G. Advani, Numerical simulations of stokes–brinkman equations for permeability prediction of dual scale fibrous porous media, Physics of Fluids 22 (11) (2010) 113101.

[28] M. Bodaghi, S. Lomov, P. Simacek, N. Correia, S. Advani, On the variability of permeability induced by reinforcement distortions and dual scale flow in liquid composite moulding: A review, Composites Part A: Applied Science and Manufacturing 120 (2019) 188–210.

[29] K. Yazdchi, S. Srivastava, S. Luding, Microstructural effects on the permeability of periodic fibrous porous media, International Journal of Multiphase Flow 37 (8) (2011) 956–966.

[30] E. Lopez, E. Abisset-Chavanne, F. Lebel, R. Upadhyay, S. Comas, C. Binetruy, F. Chinesta, Flow modeling of linear and nonlinear fluids in two and three scale fibrous fabrics, International Journal of Material Forming 9 (2) (2016) 215–227.

[31] E. Syerko, C. Binetruy, S. Comas-Cardona, A. Leygue, A numerical approach to design dual-scale porosity composite reinforcements with enhanced permeability, Materials & Design 131 (2017) 307 – 322.

[32] E. D. Luycker, Simulation of 3d interlock composite preforming, Composite Structures 88 (4) (2009) 615–623.

[33] M. V. Bruschke, S. G. Advani, Flow of generalized newtonian fluids across a periodic array of cylinders, Journal of Rheology 37 (3) (1993) 479–498.

[34] P. C. Carman, Fluid Flow Through Granular Beds, Transactions - Institution of Chemical Engineeres 15 (1937) 150–166.

[35] R. Gebart, Permeability of unidirectional reinforcements for rtm, Journal of Composite Materials 8 (26) (1992) 1100–1133.

[36] N. Vernet, F. Trochu, In-plane and through-thickness permeability models for three-dimensional Interlock fabrics, Journal of Composite Materials 50 (14) (2016) 1951–1969.

[37] Ali, M. A. and Umer, R. and Khan, K. A. and Cantwell, W. J., In-plane virtual permeability characterization of 3D woven fabrics using a hybrid experimental and numerical approach, Composites Science and Technology 173 (2019) 99–109.

[38] V. Michaud, Permeability properties of reinforcements in composites, in: P. Boisse (Ed.), Composite Reinforcements for Optimum Performance, Woodhead Publishing Limited, 2011, Ch. 14, pp. 431–457.

[39] K. L. Adams, W. B. Russel, L. Rebenfeld, Radial penetration of a viscous liquid into a planar anisotropic porous medium, International Journal of Multiphase Flow 14 (2) (1988) 203–215.

[40] P. Ferland, D. Guittard, F. Trochu, Concurrent methods for permeability measurement in resin transfer molding, Polymer composites 17 (1) (1996) 149–158.

[41] J. R. Weitzenböck, R. A. Shenoi, P. A. Wilson, Radial flow permeability measurement. part a: Theory, Composites Part A: Applied Science and Manufacturing 30 (6) (1999) 781–796.

[42] R. Gauvin, F.Trochu, Y. Lemenn, L. Diallo, Permeability measurement and flow simulation through fiber reinforcement, Polymer composites 17 (1) (1996) 34–42.

[43] D. May, A. Aktas, S. Advani, D. Berg, A. Endruweit, E. Fauster, S. Lomov, A. Long, P. Mitschang, S. Abaimov, D. Abliz, I. Akhatov, M. Ali, T. Allen, S. Bickerton, M. Bodaghi, B. Caglar, H. Caglar, A. Chiminelli, N. Correia, B. Cosson, M. Danzi, J. Dittmann, P. Ermanni, G. Francucci, A. George, V. Grishaev, M. Hancioglu, M. Kabachi, K. Kind, M. Deléglise-Lagardère, M. Laspalas, O. Lebedev, M. Lizaranzu, P.-J. Liotier, P. Middendorf, J. Morn, C.-H. Park, R. Pipes, M. Pucci, J. Raynal, E. Rodriguez, R. Schledjewski, R. Schubnel, N. Sharp, G. Sims, E. Sozer, P. Sousa, J. Thomas, R. Umer, W. Wijaya, B. Willenbacher, A. Yong, S. Zaremba, G. Ziegmann, In-plane permeability characterization of engineering textiles based on radial flow experiments: A benchmark exercise, Composites Part A: Applied Science and Manufacturing 121 (2019) 100–114.

[44] N. Vernet, E. Ruiz, S. Advani, J. Alms, M. Aubert, M. Barburski, B. Barari, J. Beraud, D. Berg, N. Correia, M. Danzi, T. Delavière, M. Dickert, C. D. Fratta, A. Endruweit, P. Ermanni, G. Francucci, J. Garcia, A. George, C. Hahn, F. Klunker, S. Lomov, A. Long, B. Louis, J. Maldonado, R. Meier, V. Michaud, H. Perrin, K. Pillai, E., F. Trochu, S. Verheyden, M. Wietgrefe, W. Xiong, S. Zaremba, G. Ziegmann, Experimental determination of the permeability of engineering textiles: Benchmark ii, Composites Part A: Applied Science and Manufacturing 61 (2014) 172–184.

[45] Salvatori, D. and Caglar, B. and Teixidó, H. and Michaud, V., Permeability and capillary effects in a channel-wise non-crimp fabric, Composites Part A: Applied Science and Manufacturing 108 (2018) 41–52.

[46] N. D. Ngo, K. K. Tamma, Microscale permeability predictions of porous fibrous media, International Journal of Heat and Mass Transfer 44 (16) (2001) 3135–3145.

[47] I. Straumit, C. Hahn, E. Winterstein, B. Plank, S. Lomov, M. Weversa, Computation of perme-

ability of a non-crimp carbon textile reinforcement based on x-ray computed tomography images, Composites Part A: Applied Science and Manufacturing 81 (2016) 289–295.

[48] B. Verleye, Computation of the permeability of multi-scale porous media with application to technical textiles, Ph.D. thesis, Katolieke Universiteit Leuven (2008).

[49] A. Vanaerschot, B. Cox, S. L. V, D. Vandepitte, Simulation of the cross-correlated positions of in-plane tow centroids in textile composites based on experimental data, Composite structures 116 (2014) 75–83.

[50] S. Lomov, G. Huysmans, Y. Luo, R. Parnas, A. Prodromou, I. Verpoest, F. Phelan, Textile composites: modelling strategies, Composites Part A: applied science and manufacturing 32 (10) (2001) 1379–1394.

[51] I. Verpoest, S. Lomov, Virtual textile composites software wisetex: Integration with micro-mechanical, permeability and structural analysis, Composites Science and Technology 65 (15-16) (2005) 2563–2574.

[52] D. Durville, Simulation of the mechanical behaviour of woven fabrics at the scale of fibers, International Journal of Material Forming 3 (2) (2010) S1241–S1251.

[53] D. Durville, I. Baydoun, H. Moustacas, G. Périé, Y. Wielhorski, Determining the initial configuration and characterizing the mechanical properties of 3d angle-interlock fabrics using finite element simulation, International Journal of Solids and Structures 154 (2018) 97–103.

[54] Ali, M. A. and Umer, R. and Khan, K. A. and Cantwell, W. J., XCT-scan assisted flow path analysis and permeability prediction of a 3D woven fabric, Composites Part B: Engineering 176 (2019) 107320.

[55] H. C. Brinkman, A calculation of the viscous force exerted by a flowing fluid on a dense swarm of particles, Applied Scientific Research 1 (1949) 27–34.

[56] E. B. Belov, S. V. Lomov, I. Verpoest, T. Peters, D. Roose, R. S. Parnas, K. Hoes, H. Sol, Modelling of permeability of textile reinforcements: lattice boltzmann method, Composites Science and Technology 64 (7) (2004) 1069 – 1080.

[57] Y. S. Song, J. R. Youn, Asymptotic expansion homogenization of permeability tensor for plain woven fabrics, Composites Part A: Applied Science and Manufacturing 37 (11) (2006) 2080 – 2087.

[58] Papathanasiou, T. D., Flow across structured fiber bundles: a dimensionless correlation, International Journal of Multiphase Flow 27 (8) (2001) 1451 – 1461.

[59] Nabovati, A. and Llewellin, E. W. and Sousa, A. C. M., Through-thickness permeability prediction of three-dimensional multifilament woven fabrics, Composites Part A: Applied Science and Manufacturing 41 (4) (2010) 453–463.

[60] L. Abouorm, M. Blais, N. Moulin, J. Bruchon, S. Drapier, A robust monolithic approach for resin infusion based process modelling, in: Key Engineering Materials, Vol. 611, Trans. Tech. Publ., 2014, pp. 306–315.

[61] L. Abouorm, N. Moulin, J. Bruchon, S. Drapier, Monolithic approach of stokes-darcy coupling for lcm process modelling, in: Key Engineering Materials, Vol. 554, Trans. Tech. Publ., 2013, pp. 447–455.

[62] L. Abouorm, R. Troian, S. Drapier, J. Bruchon, N. Moulin, StokesDarcy coupling in severe regimes using multiscale stabilisation for mixed finite elements: monolithic approach versus decoupled approach, European Journal of Computational Mechanics 23 (3-4) (2014) 113–137.

[63] M. Blais, N. Moulin, P.-J. Liotier, S. Drapier, Resin infusion-based processes simulation : coupled Stokes-Darcy flows in orthotropic preforms undergoing finite strain, International Journal of Material Forming 10 (1) (2017) 43–54.

[64] G. Pacquaut, J. Bruchon, N. Moulin, S. Drapier, Combining a level-set method and a mixed stabilized p1/p1 formulation for coupling stokes–darcy flows, International Journal for Numerical Methods in Fluids 69 (2) (2012) 459–480.

[65] Z. set Software, http://www.zset-software.com/.

[66] T. J. R. Hughes, Multiscale phenomena: Green's functions, the Dirichlet-to-Neumann formulation, subgrid scale models, bubbles and the origins of stabilized methods, Computer methods in applied mechanics and engineering 127 (1) (1995) 387–401.

[67] S. Badia, R. Codina, Unified stabilized finite element formulations for the stokes and the darcy problems, SIAM journal on Numerical Analysis 47 (3) (2009) 1971–2000.

[68] J. B. Keller, Viscous flow through a grating or lattice of cylinders, Journal of fluid mechanics 18 (1) (1964) 94–96.

[69] D. Durville, Modélisation du comportement mécanique des câbles métalliques, Revue Européenne des Éléments Finis 7 (1–3) (1998) 9–22.

[70] D. Durville, Modélisation par éléments finis du comportement mécanique de structures textiles : de la fibre au tissu, Revue Européenne des Éléments Finis 11 (2–4) (2002) 463–477.

[71] G. S. Beavers, D. D. Joseph, Boundary conditions at a naturally permeable wall, Journal of Fluid Mechanics 30 (01) (1967) 197–207.

[72] P. Celle, S. Drapier, J.-M. Bergheau, Numerical modelling of liquid infusion into fibrous media undergoing compaction, European Journal of Mechanics - A/Solids 27 (4) (2008) 647–661.

[73] A. Dereims, S. Drapier, J.-M. Bergheau, P. de Luca, 3d robust iterative coupling of Stokes, Darcy and solid mechanics for low permeability media undergoing finite strains, Finite Elements in Analysis and Design 94 (2015) 1–15.

[74] X. Chen, T. D. Papathanasiou, The transverse permeability of disordered fiber arrays: a statistical correlation in terms of the mean nearest interfiber spacing, Transport in Porous Media 71 (2) (2008) 233–251.

[75] K. Yazdchi, S. Srivastava, S. Luding, Micro–macro relations for flow through random arrays of cylinders, Composites Part A: Applied Science and Manufacturing 43 (11) (2012) 2007–2020.

[76] P. R. Amestoy, I. S. Duff, J. Koster, J.-Y. L'Excellent, A fully asynchronous multifrontal solver using distributed dynamic scheduling, SIAM Journal on Matrix Analysis and Applications 23 (1) (2001) 15–41.

[77] Xiao, X. and Endruweit, A. and Zeng, X. and Hu, J. and Long, A., Through-thickness permeability study of orthogonal and angle-interlock woven fabrics, Journal of Materials Science 50 (3) (2015) 1257–1266.

[78] Pucci M. F. and Duchemin B. and Gomina M. and Bréard J., Temperature effect on dynamic wetting of cellulosic substrates by molten polymers for composite processing, Composites Part A: Applied Science and Manufacturing 114 (2018) 307 – 315.

[79] Wielhorski Y. and Abdelwahed A. B. and Arquis E. and Glockner S. and Bréard J., Numerical simulation of bubble formation and transport in cross-flowing streams, The Journal of Computational Multiphase Flows 6 (3) (2014) 299–312.

[80] Y. Wielhorski and M. A. Ben Abdelwahed and L. Bizet and J. Bréard, Wetting effect on bubble shapes formed in a cylindrical t-junction, Chemical Engineering Science 84 (2012) 100 – 106.

[81] Andriamananjara, K. and Moulin, N. and Bruchon, J. and Liotier, P.-J. and Drapier, S., Numerical modeling of local capillary effects in porous media as a pressure discontinuity acting on the interface of a transient bi-fluid flow, International Journal of Material Forming 12 (4) (2019) 675–691.

[82] Pucci, M. F. and Liotier, P.-J. and Drapier, S., Capillary wicking in a fibrous reinforcement Orthotropic issues to determine the capillary pressure components, Composites Part A: Applied Science and Manufacturing 77 (2015) 133–141.